



Regular article

Evaluation of coating thickness by thermal wave imaging: A comparative study of pulsed and lock-in infrared thermography – Part II: Experimental investigation

Ranjit Shrestha, Wontae Kim*

Department of Mechanical & Automotive Engineering, Kongju National University, 1223-24 Cheonan-daero, Seobuk-gu, Cheonan-si, Chungcheongnam-do 31080, South Korea



ARTICLE INFO

Keywords:

Thermal barrier coatings
Topcoat thickness measurement
Thermal wave imaging
Pulsed thermography
Lock-in thermography
Fourier transform
Phase angle

ABSTRACT

In this work, we focused on the experimental arrangement of thermal wave imaging (TWI) methods for the quantitative evaluation of non-uniform topcoat thickness of thermal barrier coatings (TBCs). Two TWI techniques, pulsed thermography (PT) and lock-in thermography (LIT) were implemented on plasma sprayed TBCs with varied topcoat ranging from 0.1 mm to 0.6 mm. In PT, a short and high energy light pulse was applied on a sample surface whereas, in LIT, the sample surface was excited by a sinusoidal heat flux at several modulation frequencies ranging from 2 Hz down to 0.01 Hz. Furthermore, an infrared camera was used to capture the surface temperature of a thermal wave that propagated into the sample and the effect of the applied heat flux in both techniques was analyzed by Fourier transform. The results of PT and LIT techniques were compared based on the evaluated accuracy of each technique. Finally, it was concluded that both the techniques could be applied to the fast and accurate evaluation of TBCs thickness.

1. Introduction

Thermal barrier coatings (TBCs) are complex, multifunctional thick films of a refractory-oxide ceramic applied to the metallic surfaces of hot section components to protect from wear, erosion and high-temperature degradation, and to provide thermal insulation [1–3]. TBCs are now being used to provide thermal insulation to metallic components from the hot gas stream in gas-turbine engines used for aircraft propulsion, power generation, and marine propulsion [4–6]. The state-of-the-art TBCs consist of a yttria stabilized zirconia (YSZ) top coat, a thin thermally grown oxide (TGO) reaction layer and a metallic bond coat of MCrAlY on a superalloy substrate. The thermal insulation is provided by the topcoat YSZ layer deposited by either electron beam physical vapor deposition (EB-PVD) or plasma-spraying (PS) techniques [7–10]. Hence, the topcoat thickness is an essential parameter which determines the thermal insulation characteristics, stress, bonding strength, lifetime of components, costs, etc., and is important for performance evaluation [11–13]. Therefore, there is a need for non-destructive testing (NDT) techniques to monitor and control the thickness of coating.

Over the years, a variety of NDT techniques such as eddy current [14–17], ultrasonic [18–21], x-ray fluorescence [22–25], and terahertz

[26–28] has been developed for the evaluation of coatings. The choice among these techniques depends on the type of coatings, coating thickness, the substrate, the cost of instrumentation and the accuracy required [29,30]. However, these all have certain limitations such as; eddy current suffers from manual scanning; ultrasonic suffers from size and shape of the target object; x-ray is difficult to competent due to porous nature of TBCs and terahertz suffers from the requirement of a refractive index [31–34]. In this context, thermal wave imaging (TWI) often known as infrared thermography (IR) becomes a research hotspot in recent years as it has unique advantages of large detection area, fast speed, non-contact, safe and convenient operation, more coating materials and high efficiency over other inspection methods [6,35–37]. Pulsed thermography (PT) [38–42] and lock-in thermography (LIT) [43–47] are proved to be very appropriate NDT techniques for the evaluation of TBCs [48–52].

In our previous work, hereafter Part I [53], results of a systematic investigation of non-uniform TBCs using finite element model (FEM) analysis were reported. In part I, a transient FEM model was developed in ANSYS heat transfer module and stimulated by a flow of heat to simulate PT and LIT experimental procedures. The sample considered for the analysis was characterized by a steady substrate and the bond coat with varied topcoat ranging from 0.1 mm to 0.6 mm. The response

* Corresponding author.

E-mail address: kwt@kongju.ac.kr (W. Kim).

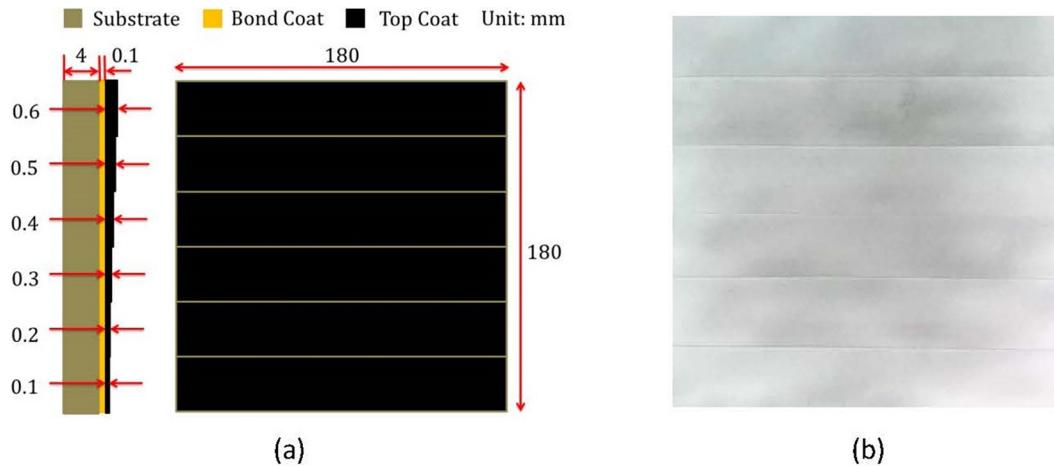


Fig. 1. TBCs test sample description, (a) Schematic illustration of the sample along with the geometry and (b) Front side of the sample.

of the thermally excited surface was recorded and analyzed by Fourier transform (FT) [54–56]. As results, we found that FEM enabled a better understanding of PT and LIT and demonstrated potential in the evaluation of TBCs thickness. In order to extend our previous study and to validate the FEM analysis results, we focused on the experimental arrangement of PT and LIT techniques. In this work, we present the experimental results and discuss them together with the results from Part I.

2. Materials and methods

2.1. Sample

Fig. 1 shows the schematic illustration of TBCs test sample along with the geometry and the front side of the sample. Nickel-based superalloy ($180 \times 180 \times 4$, in mm) plate was used a substrate. MCrAlY alloys ($M = \text{Co}, \text{Ni}, \text{or Co/Ni}$) powder by air plasma spraying (APS) process was sprayed onto the top surface of the substrate to form a bond coat of 0.1 mm. Then topcoat of Ytria-stabilized zirconia (YSZ) by APS process was applied to the bond coat surface. The thickness of topcoat was maintained in the range of 0.1–0.6 mm as shown in Fig. 1. The emissivity of YSZ-TBCs was measured and is about 0.73 [57]. The details of nanomaterials used for the preparation of TBCs can be found in the literature [58–61].

2.2. Pulse thermography (PT) experimental system

The PT system consisted of the power system, flash lamp, an infrared (IR) camera and a system controller. A power supply (BALCAR Light System, Nexus A 6400, France) utilized a flash lamp (Universal BALCAR, France) of power 6400 W-s as a heat source to launch a pulse of heat into the specimen surface. An IR camera (SC645, FLIR Systems, Sweden) with a 640×480 – pixel resolution and a wavelength of 7.5–13 μm was used to record the thermal response of the sample. An IR lens with focal length 41.3 mm was used together with the camera, which was positioned in such a way that it would fully capture the entire sample. The FLIR R&D software was used to acquire the thermal images. The camera frame rate was set to 50 frames per second.

2.3. Lock-in thermography (LIT) experimental system

The LIT system consisted of a lock-in module, a heat source, an IR camera, and a system controller [62–64]. A programmable function generator (Agilent 33210A, Malaysia) was used for the generation of sine waves. Two halogen lamps (OSRAM, Medium Flood, China) of 1 kW each were used as a heat source. The LIT system (Answer Tech,

Republic of Korea) was used to synchronize the input and output signals. The same infrared camera as specified in PT experimental system was used for LIT experimental investigation.

3. Results and discussions

3.1. PT results

The PT experimental investigation was conducted in reflection mode. The pulse heating time was set as 10 ms followed by cooling time of 5 s. Fig. 2 shows the surface temperature responses of TBCs with respect to variation in thickness of topcoat. During the measurement of temperature, a region of interest (ROI) was selected, and the temperature of each pixel within the ROI was averaged to reduce the noise and the errors in the measurement. Fig. 3 shows the pulsed thermal images acquired at a different time interval. As can be seen in Figs. 2 and 3, the temperature rise was faster than its decay because of very short impulse time. As the time passes, due to thermal diffusion in all directions, the temperature on the sample surface tended to reach equilibrium. It was also observed that the surface temperature was relatively high at large thickness.

The whole thermal data were processed by FT to compute phase angle. Fig. 4 shows the computed phase image and Fig. 5 shows the plot of phase angle with respect to variation in topcoat thickness. As can be seen in Figs. 4 and 5, phase angle decreased with the increasing coating thickness. However, notably in Part I, the phase angle increased with

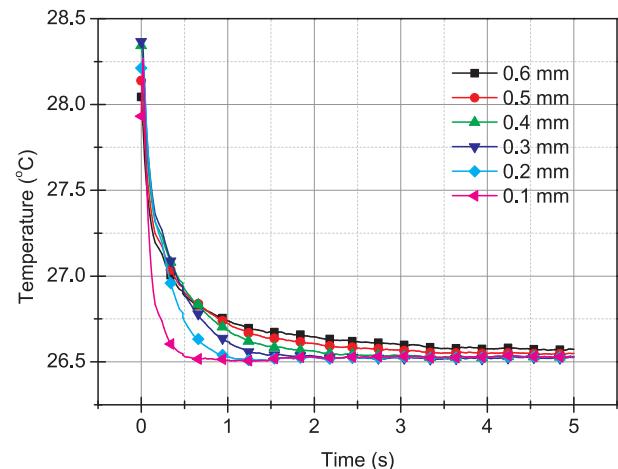


Fig. 2. PT Experimental surface temperature evolution curves of TBCs with respect to variation in the thickness of topcoat.

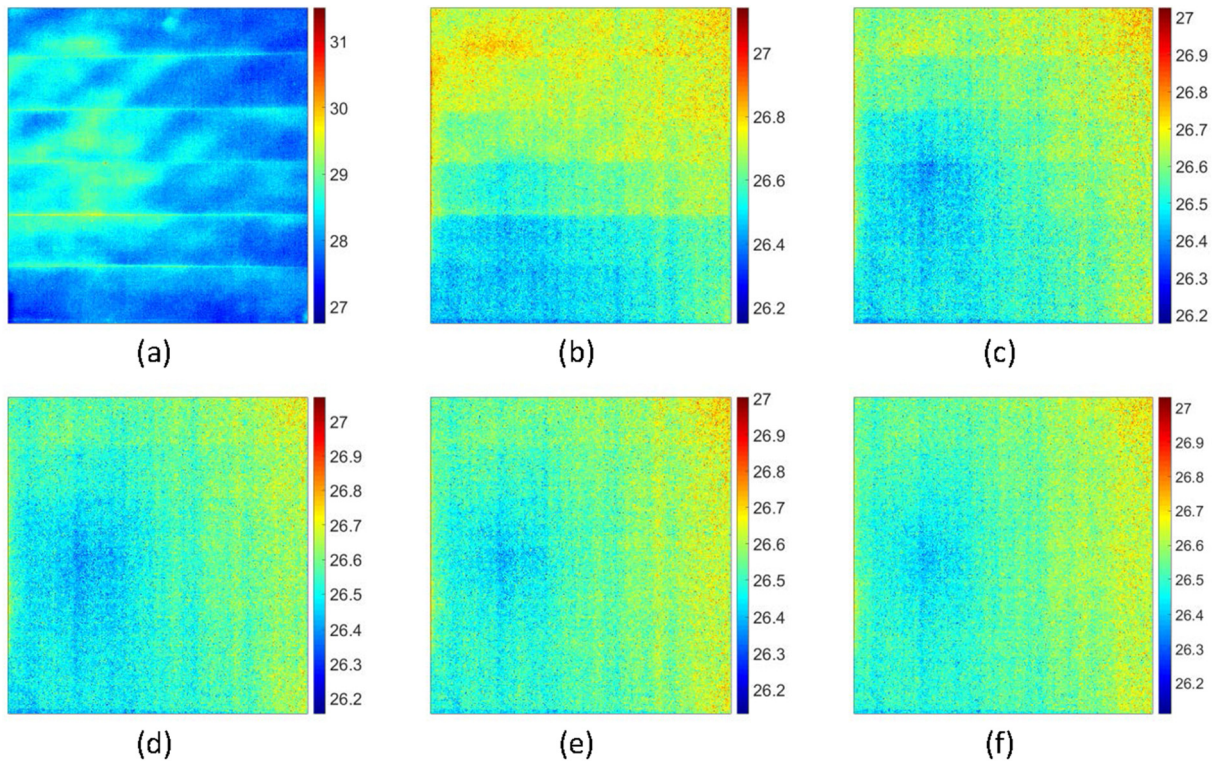


Fig. 3. PT Experimental thermal images at different time interval, (a) time 0.01 s, (b) time 1 s, (c) time 2 s, (d) time 3 s, (e) time 4 s and (f) time 5 s.

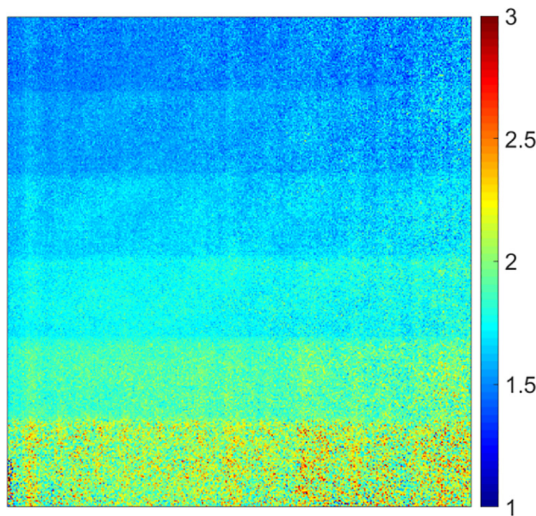


Fig. 4. Phase image processed with FT from the experimental PT data.

increasing coating thickness. It is due to the reason that the phase angle computed with FT strongly depends on the number of thermal images in sequence (number of harmonic) considered during processing. We would like to emphasize the number of harmonic considered in Part I was two, while all the thermal images of a sequence were considered in this study.

The quadratic fitting with R-Square (R^2) = 0.9976 and adj. R-Square (aR^2) = 0.9960 was adopted to express coating thickness as a function of phase angle and is expressed as Eq. (1),

$$T = 5.5418 - 3.2137\phi + 0.4522\phi^2 \quad (1)$$

3.2. LIT results

The LIT experimental investigation was conducted in reflection

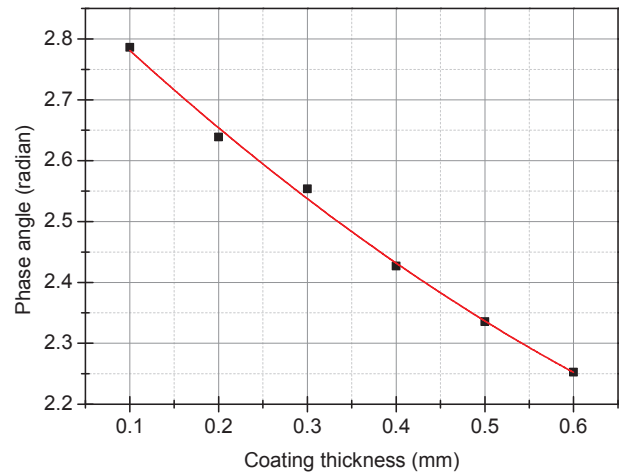


Fig. 5. Plot of coating thickness and phase angle for PT.

mode for three complete excitation cycles at modulation frequencies of 2 Hz, 1 Hz, 0.5 Hz, 0.2 Hz, 0.1 Hz, 0.05 Hz, 0.02 Hz and 0.01 Hz. The recorded thermal data from the 2nd excitation cycle was processed by FT to compute phase angle for all the excitation frequencies. Fig. 6 shows the computed phase angle image. Fig. 7 shows the plot of coating thickness and phase angle as a function of excitation frequency. As can be seen in Figs. 6 and 7, phase angle decreased with the increasing coating thickness. It was also found that the most appropriate excitation frequency was found to be 0.02 Hz, since the higher phase difference was obtained at this frequency. Hence, phase angle image at 0.02 Hz was considered for the further analysis.

The quadratic fitting with R-Square (R^2) = 0.9504 and adj. R-Square (aR^2) = 0.91642 was adopted to express coating thickness as a function of phase angle and is expressed as Eq. (2),

$$T = 0.30247 - 0.14977\phi - 0.01039\phi^2 \quad (2)$$

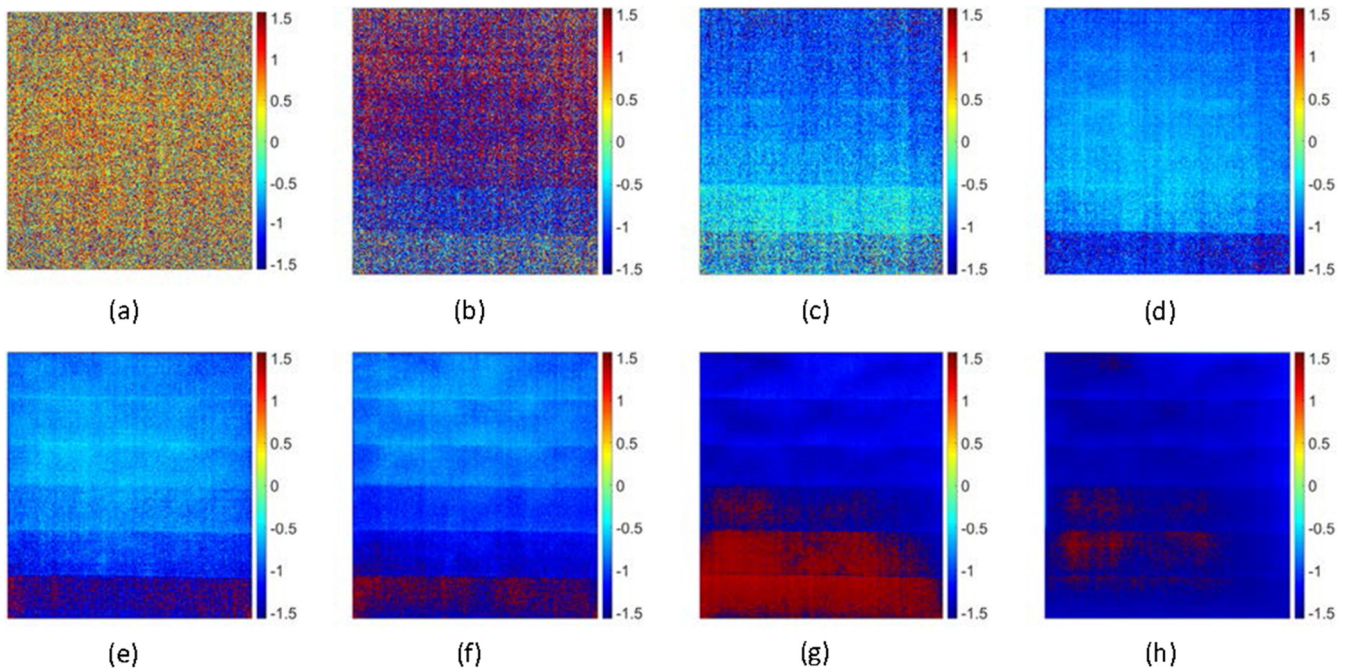


Fig. 6. Phase images processed with the FT from the LIT experimental data at different modulation frequencies: (a) 2 Hz, (b) 1 Hz, (c) 0.5 Hz, (d) 0.2 Hz, (e) 0.1 Hz, (f) 0.05 Hz, (g) 0.02 Hz and (h) 0.01 Hz.

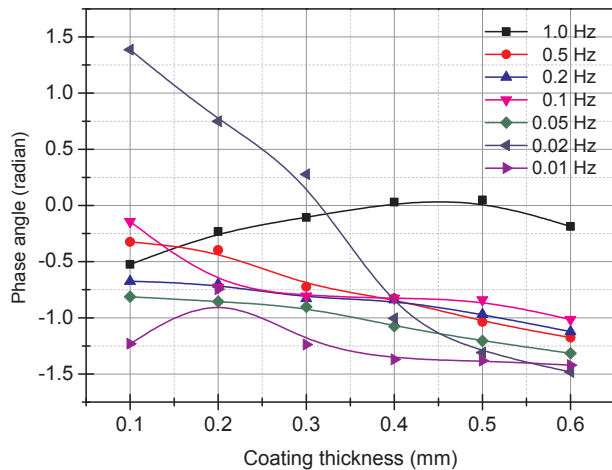


Fig. 7. Plot of coating thickness and phase angle as a function of modulation frequency for LIT.

3.3. Comparison of PT and LIT

The details of evaluated phase angle, predictive thickness and percentage error for each technique are summarized in Table 1. As can be seen in Table 1, results indicate that phase angle decreased with the

Table 1
Predicted coating thickness and error percentage.

Actual thickness (T) (mm)	Pulsed thermography			Lock-in thermography		
	Calculated ϕ (radian)	Predictive t (mm)	Error (%)	Calculated ϕ (radian)	Predictive t (mm)	Error (%)
0.6	2.2527	0.5971	0.49	-1.4817	0.5485	8.58
0.5	2.3356	0.5026	0.52	-1.2944	0.5148	2.96
0.4	2.4268	0.4060	1.49	-1.0044	0.4641	16.01
0.3	2.5537	0.2839	5.35	0.2768	0.2617	12.77
0.2	2.6388	0.2103	5.14	0.7490	0.1960	1.98
0.1	2.7859	0.0984	1.65	1.3857	0.1151	15.14

increasing coating thickness for both PT and LIT techniques. The thickness of the varied topcoat was evaluated by using Eqs. (1) and (2) respectively for PT and LIT techniques. The percentage error was calculated for the evaluated thickness. Results revealed that PT was found to be more accurate than to LIT. However, error present in both techniques was satisfactory and within the acceptable limit.

4. Conclusions

We supplemented our previous FEM analysis results on quantitative evaluation of non-uniform TBCs thickness with new experimental results. The new experimental results together with the previous results (Part I) showed that both the PT and LIT techniques could be applied to the fast and accurate evaluation of TBCs thickness. It was found that the differences in the temperature of thermal image and its corresponding phase angle played a significant role in the evaluation of TBCs thickness. PT and LIT technique were compared with each other based on the evaluated accuracy of each technique. PT was found to be faster and more accurate as compared to LIT. Particularly, for LIT, several excitation frequencies ranging from 2 Hz down to 0.01 Hz were explored, and it was found that a frequency of 0.02 Hz provided a good result.

Conflict of interest

The authors declared that there is no conflict of interest.

Acknowledgment

This work was supported by National Research Foundation of Korea (NRF-2016R1D1A1B03932587) funded by Ministry of Education, Science and Technology, Republic of Korea and by the Human Resources Development program (No. 20154030200940) of the Korea Institute of Energy Technology Evaluation and Planning (KETEP) grant funded by the Ministry of Trade, Industry and Energy, Republic of Korea.

Appendix A. Supplementary material

Supplementary data associated with this article can be found, in the online version, at <https://doi.org/10.1016/j.infrared.2018.05.001>.

References

- [1] D.R. Clarke, S.R. Phillpot, Thermal barrier coating materials, *Mater. Today* 8 (6) (2005) 22–29.
- [2] D.R. Clarke, M. Oechsner, N.P. Padture, Thermal-barrier coatings for more efficient gas-turbine engines, *MRS Bull.* 37 (10) (2012) 891–898.
- [3] B. Rogé, A. Fahr, J. Giguere, K. McRae, Nondestructive measurement of porosity in thermal barrier coatings, *J. Therm. Spray Technol.* 12 (4) (2003) 530–535.
- [4] N.P. Padture, M. Gell, E.H. Jordan, Thermal barrier coatings for gas-turbine engine applications, *Science* 296 (5566) (2002) 280–284.
- [5] X. Song, F. Meng, M. Kong, Y. Wang, L. Huang, X. Zheng, Y. Zeng, Thickness and microstructure characterization of TGO in thermal barrier coatings by 3D reconstruction, *Mater. Charact.* 120 (2016) 244–248.
- [6] Q. Tang, J. Dai, C. Bu, L. Qi, D. Li, Experimental study on debonding defects detection in thermal barrier coating structure using infrared lock-in thermographic technique, *Appl. Therm. Eng.* 107 (2016) 463–468.
- [7] G. Chen, Non-destructive evaluation (NDE) of the failure of thermal barrier coatings, *Therm. Barrier Coat.* (2011) 243–262.
- [8] T. Fukuchi, T. Ozeki, M. Okada, T. Fujii, Nondestructive inspection of thermal barrier coating of gas turbine high temperature components, *IEEE Trans. Electr. Electron. Eng.* 11 (4) (2016) 391–400.
- [9] S. Sampath, U. Schulz, M.O. Jarligo, S. Kuroda, Processing science of advanced thermal-barrier systems, *MRS Bull.* 37 (10) (2012) 903–910.
- [10] D. Zhu, R.A. Miller, Thermal-barrier coatings for advanced gas-turbine engines, *MRS Bull.* 25 (7) (2000) 43–47.
- [11] D.M. Nissley, Thermal barrier coating life modeling in aircraft gas turbine engines, *J. Therm. Spray Technol.* 6 (1) (1997) 91.
- [12] T. Fukuchi, N. Fuse, M. Okada, T. Ozeki, T. Fujii, M. Mizuno, K. Fukunaga, Topcoat thickness measurement of thermal barrier coating of gas turbine blade using terahertz wave, *Electr. Eng. Jpn.* 189 (1) (2014) 1–8.
- [13] L. Wang, X. Zhong, Y. Zhao, S. Tao, W. Zhang, Y. Wang, X. Sun, Design and optimization of coating structure for the thermal barrier coatings fabricated by atmospheric plasma spraying via finite element method, *J. Asian Ceram. Soc.* 2 (2) (2014) 102–116.
- [14] H. Yang, C. Tai, Pulsed eddy-current measurement of a conducting coating on a magnetic metal plate, *Meas. Sci. Technol.* 13 (8) (2002) 1259.
- [15] W. Yin, A. Peyton, Thickness measurement of non-magnetic plates using multi-frequency eddy current sensors, *NDT E Int.* 40 (1) (2007) 43–48.
- [16] J. Zhang, M. Yuan, S. Song, H. Kim, Precision measurement of coating thickness on ferromagnetic tube using pulsed eddy current technique, *Int. J. Precis. Eng. Manuf.* 16 (8) (2015) 1723–1728.
- [17] D. Zhang, Y. Yu, C. Lai, G. Tian, Thickness measurement of multi-layer conductive coatings using multifrequency eddy current techniques, *Nondestruct. Test Eval.* 31 (3) (2016) 191–208.
- [18] A.I. Lavrentyev, S.I. Rokhlin, An ultrasonic method for determination of elastic moduli, density, attenuation and thickness of a polymer coating on a stiff plate, *Ultrasonics* 39 (3) (2001) 211–221.
- [19] S. Dixon, B. Lanyon, G. Rowlands, Coating thickness and elastic modulus measurement using ultrasonic bulk wave resonance, *Appl. Phys. Lett.* 88 (14) (2006) 141907.
- [20] Y. Zhao, L. Lin, X. Li, M. Lei, Simultaneous determination of the coating thickness and its longitudinal velocity by ultrasonic nondestructive method, *NDT E Int.* 43 (7) (2010) 579–585.
- [21] H.R. Chen, B. Zhang, M.A. Alvin, Y. Lin, Ultrasonic detection of delamination and material characterization of thermal barrier coatings, *J. Therm. Spray Technol.* 21 (6) (2012) 1184–1194.
- [22] S. Jain, P. Gupta, A. Eapen, An X-ray fluorescence method for coating thickness measurement, *X-Ray Spectrom.* 8 (1) (1979) 11–13.
- [23] M. Kolbe, B. Beckhoff, M. Krumrey, G. Ulm, Thickness determination for Cu and Ni nanolayers: Comparison of completely reference-free fundamental parameter-based X-ray fluorescence analysis and X-ray reflectometry, *Spectrochim. Acta Part B: Atomic Spectrosc.* 60 (4) (2005) 505–510.
- [24] A. Carapelle, K. Fleury-Frenette, J. Collette, H. Garnir, P. Harlet, Portable x-ray fluorescence spectrometer for coating thickness measurement, *Rev. Sci. Instrum.* 78 (12) (2007) 123109.
- [25] I. Queral, J. Ibañez, E. Margu, J. Pujol, Thickness measurement of semiconductor thin films by energy dispersive X-ray fluorescence benchtop instrumentation: Application to GaN epilayers grown by molecular beam epitaxy, *Spectrochim. Acta Part B: Atomic Spectrosc.* 65 (7) (2010) 583–586.
- [26] J. White, G. Fichter, A. Chernovsky, J.F. Whitaker, D. Das, T.M. Pollock, D. Zimdars, Time domain terahertz non-destructive evaluation of aeroturbine blade thermal barrier coatings, vol. 1096, No. 1, 2009, pp. 434–439.
- [27] C. Chen, D. Lee, T. Pollock, J.F. Whitaker, Pulsed-terahertz reflectometry for health monitoring of ceramic thermal barrier coatings, *Opt. Express* 18 (4) (2010) 3477–3486.
- [28] T. Fukuchi, N. Fuse, M. Okada, T. Fujii, M. Mizuno, K. Fukunaga, Measurement of refractive index and thickness of topcoat of thermal barrier coating by reflection measurement of Terahertz waves, *Electron. Commun. Jpn.* 96 (12) (2013) 37–45.
- [29] M. Aoyagi, T. Hiraguri, T. Ueno, Nondestructive analysis of uneven paint coatings by dynamic heat conduction following flash heating, *J. Coat. Technol. Res.* 11 (3) (2014) 311–318.
- [30] S. Mezghani, E. Perrin, V. Vrabie, J. Bodnar, J. Marthe, B. Cauwe, Evaluation of paint coating thickness variations based on pulsed Infrared thermography laser technique, *Infrared Phys. Technol.* 76 (2016) 393–401.
- [31] National Research Council, Coatings for high-temperature structural materials: trends and opportunities, 1996.
- [32] P.G. Bison, S. Marinetti, E.G. Grinzato, V.P. Vavilov, F. Cernuschi, D. Robba, Inspecting thermal barrier coatings by IR thermography, vol. 5073, 2003, pp. 318–328.
- [33] S. Mezghani, E. Perrin, J. Bodnar, J. Marthe, B. Cauwe, V. Vrabie, Evaluation of heterogeneity of paint coating on metal substrate using laser infrared thermography and eddy current, *World Acad. Sci., Eng. Technol. Int. J. Civ. Environ. Eng.* 2 (5) (2015).
- [34] Q. Tang, J. Liu, J. Dai, Z. Yu, Theoretical and experimental study on thermal barrier coating (TBC) uneven thickness detection using pulsed infrared thermography technology, *Appl. Therm. Eng.* 114 (2017) 770–775.
- [35] X. Maldague, Applications of infrared thermography in nondestructive evaluation, *Trends Opt. Nondestruct. Test.* (2000) 591–609.
- [36] X.P. Maldague, Introduction to NDT by active infrared thermography, *Mater. Eval.* 60 (9) (2002) 1060–1073.
- [37] C. Bu, Q. Tang, Y. Liu, F. Yu, C. Mei, Y. Zhao, Quantitative detection of thermal barrier coating thickness based on simulated annealing algorithm using pulsed infrared thermography technology, *Appl. Therm. Eng.* 99 (2016) 751–755.
- [38] X. Maldague, S. Marinetti, Pulse phase infrared thermography, *J. Appl. Phys.* 79 (5) (1996) 2694–2698.
- [39] X. Maldague, F. Galmiche, A. Ziadi, Advances in pulsed phase thermography, *Infrared Phys. Technol.* 43 (3–5) (2002) 175–181.
- [40] C. Ibarra-Castaneda, X. Maldague, Pulsed phase thermography reviewed, *Quantit. Infrared Thermography J.* 1 (1) (2004) 47–70.
- [41] V.P. Vavilov, D.D. Burleigh, Review of pulsed thermal NDT: Physical principles, theory and data processing, *NDT E Int.* 73 (2015) 28–52.
- [42] R. Shrestha, W. Kim, Modelling of pulse thermography for defect detection in aluminium structures: Assessment on reflection and transmission measurement, *World J. Modell. Simul.* 13 (1) (2017) 45–51.
- [43] D. Wu, J. Rantala, W. Karpen, G. Zenzinger, R. Schönbach, W. Rippel, R. Stegmüller, L. Diener, G. Busse, *Appl. Lockin-thermography Methods* (1996) 511–518.
- [44] D. Wu, G. Busse, Lock-in thermography for nondestructive evaluation of materials, *Revue générale de Thermique* 37 (8) (1998) 693–703.
- [45] X. Maldague, P.O. Moore, *Nondestructive testing handbook: infrared and thermal testing*, 2001.
- [46] X. Maldague, *Theory and practice of infrared technology for nondestructive testing*, 2001.
- [47] M. Choi, K. Kang, J. Park, W. Kim, K. Kim, Quantitative determination of a subsurface defect of reference specimen by lock-in infrared thermography, *NDT E Int.* 41 (2) (2008) 119–124.
- [48] J. Liu, Q. Tang, Y. Wang, J. Gong, L. Qin, Investigation on Coating Uniformity of High-Temperature Alloy with SiC Thermal Barrier Coating Using Pulsed Infrared Thermographic Technique, *Int. J. Thermophys.* 36 (5–6) (2015) 1252–1258.
- [49] D. Palumbo, R. Tamborrino, U. Galietti, Coating defect evaluation based on stimulated thermography, vol. 10214, 2017, 102140X.
- [50] S. Marinetti, V. Vavilov, P. Bison, E. Grinzato, F. Cernuschi, Quantitative infrared thermographic nondestructive testing of thermal barrier coating, *Mater. Eval.* (2003).
- [51] J. Zhang, L. Wu, Research on measurement of thickness and damage degree of coatings based on lock-in thermography, vol. 100, No. 1, 2017, pp. 012043.
- [52] J. Zhang, X. Meng, Y. Ma, A new measurement method of coatings thickness based on lock-in thermography, *Infrared Phys. Technol.* 76 (2016) 655–660.
- [53] R. Shrestha, W. Kim, Evaluation of coating thickness by thermal wave imaging: A comparative study of pulsed and lock-in infrared thermography—Part I: Simulation, *Infrared Phys. Technol.* 83 (2017) 124–131.
- [54] R.N. Bracewell, R.N. Bracewell, *The Fourier transform and its applications*, vol. 31999, 1986.
- [55] R.B. Randall, *Frequency analysis*, 1987.
- [56] C. Ibarra-Castaneda, D. Gonzalez, M. Klein, M. Pilla, S. Vallerand, X. Maldague, Infrared image processing and data analysis, *Infrared Phys. Technol.* 46 (1–2) (2004) 75–83.
- [57] S.D. Alaruri, L. Bianchini, A. Brewington, Emissivity measurements for YSZ thermal barrier coating at high temperatures using a 1.6- μm single-wavelength pyrometer, *Opt. Eng.* 37 (2) (1998) 683–688.
- [58] R.S. Razavi, M.R. Lohman-Estarki, *Advance Techniques for the Synthesis of Nanostructured Zirconia-Based Ceramics for Thermal Barrier Application*, 2017, pp.

- 21–91.
- [59] S. Zinatloo-Ajabshir, M. Salavati-Niasari, Facile synthesis of nanocrystalline neodymium zirconate for highly efficient photodegradation of organic dyes, *J. Mol. Liq.* 243 (2017) 219–226.
- [60] S. Zinatloo-Ajabshir, Z. Zinatloo-Ajabshir, M. Salavati-Niasari, S. Bagheri, S.B.A. Hamid, Facile preparation of $\text{Nd}_2\text{Zr}_2\text{O}_7\text{-ZrO}_2$ nanocomposites as an effective photocatalyst via a new route, *J. Energy Chem.* 26 (2) (2017) 315–323.
- [61] S. Zinatloo-Ajabshir, M. Salavati-Niasari, Photo-catalytic degradation of erythrosine and eriochrome black T dyes using $\text{Nd}_2\text{Zr}_2\text{O}_7$ nanostructures prepared by a modified Pechini approach, *Sep. Purif. Technol.* 179 (2017) 77–85.
- [62] R. Shrestha, J. Park, W. Kim, Application of thermal wave imaging and phase shifting method for defect detection in Stainless steel, *Infrared Phys. Technol.* 76 (2016) 676–683.
- [63] S. Ranjit, K. Kang, W. Kim, Investigation of lock-in infrared thermography for evaluation of subsurface defects size and depth, *Int. J. Precis. Eng. Manuf.* 16 (11) (2015) 2255–2264.
- [64] S. Ranjit, M. Choi, W. Kim, Quantification of defects depth in glass fiber reinforced plastic plate by infrared lock-in thermography, *J. Mech. Sci. Technol.* 30 (3) (2016) 1111–1118.